Hybrid Materials Based on ZnO Nanoparticles and Organo-Modified Silica Coatings as Eco-Friendly Anticorrosive Protection for Metallic Historic Artifacts

Mihaela Ioan [1], Dan Florin Anghel [1], Mihai Anastasescu [1], Ioana Catalina Gifu [2], Elvira Alexandrescu [2], Roxana Ioana Matei [2,3], Cristian Petcu [2,*], Ioana Stanculescu [4,5], Georgiana Alexandra Sanda [5], Daniela Bala [5] and Ludmila Otilia Cinteza [5,*]

1   "Ilie Murgulescu" Institute of Physical Chemistry, Romanian Academy, 202 Spl. Independentei, 060021 Bucharest, Romania
2   Polymer Department, National Institute for Research and Development in Chemistry and Petrochemistry—ICECHIM, 202 Spl. Independentei, 060021 Bucharest, Romania
3   Faculty of Chemical Engineering and Biotechnologies, University "Politehnica" of Bucharest, 060042 Bucharest, Romania
4   IRASM Department, Horia Hulubei National Institute for Physics and Nuclear Engineering, 30 Reactorului Str., 077125 Magurele, Romania
5   Physical Chemistry Department, University of Bucharest, 4–12 Blv. Regina Elisabeta, 030018 Bucharest, Romania
*   Correspondence: cpetcu@icf.ro (C.P.); ocinteza@gw-chimie.math.unibuc.ro (L.O.C.)

Abstract: Cultural heritage metallic artifacts are often subjected to environmental factors that promote degradation through corrosion processes. Anticorrosion protection is needed both for the long-term preservation of outdoor monuments and the short-term conservation of archaeological artifacts. In this work, functional nanocoatings based on ZnO nanoparticles (NPs) in a silica matrix are prepared as a replacement for a commercial Incralac lacquer. Facile sol–gel synthesis is employed for obtaining silica filmogenic materials, using tetraethoxysilane (TEOS) and 3-glycidyloxypropyl trimethoxysilane (GPTMS). Silica-based nanocomposite coatings, with and without ZnO NPs and benzotriazole (BTA) as anticorrosion agents, applied on copper coupons by brushing are characterized by using VIS and FTIR spectroscopy, SEM and AFM and compared to Incralac lacquer as reference materials. The optical and morphological properties of the proposed silica coatings are similar to the Incralac specimens. The protective effect against corrosion is investigated on the copper coupons as model metallic objects subjected to a corrosion test by using potentiodynamic polarization in a 3.5% NaCl solution at ambient temperature. The influence of the presence of BTA and ZnO NPs in both silica and Incralac coatings is studied, and the variations in the anticorrosive, morphological and optical properties with the concentration of ZnO NPs are evidenced. The presence of moderate concentrations of ZnO in both nanomaterials leads to changes in the color parameters slightly above the limit accepted in the field of cultural heritage (ΔE^* 5.09 and 6.13), while a high ZnO concentration of 3% leads to higher values ($\Delta E^* > 10$). Regarding the anticorrosive effect, the silica-based coatings with ZnO and BTA present similar efficiencies to that of the Incralac reference material (corrosion rates in the range of 0.044–0.067 mm/year for silica coatings compared to 0.055 mm/year for Incralac).

Keywords: anticorrosive protection; functional coating; ZnO nanoparticles; silica films; cultural heritage

1. Introduction

Protecting artistic and historical objects from corrosion is an important goal in the process of restoring and preserving cultural heritage. Copper and its alloys have been frequently used to fabricate objects during the entire human history; thus, many archaeological artifacts are targeted for conservation interventions, both for long-term protection or

during restoration, as a temporary protective coating, to ensure the stability of the freshly dug-up artifact [1,2].

Corrosion, the process of a gradual deterioration of metal caused by chemical reactions, is a major threat to the conservation of metallic objects. Several methods are currently used to reduce the corrosion of metallic objects, such as the following: (i) protective coatings [3,4]; (ii) storage in a controlled environment; (iii) electrochemical methods [5]; and (iv) the microbial inhibition of corrosion [6].

However, the choice of method and material for the anticorrosion treatment of metallic objects, when applied to cultural heritage monuments or historical works of art, is subject to particular requirements imposed by the specificity of a domain. These requirements are mainly related to the reversibility and the lack of modification of the appearance of the treated object [7]. The common way in the conservation field is protection with coating materials, and in recent years, a significant amount of research has been devoted to the development of novel materials, with superior efficiency, designed for application on historic artifacts [8,9]. Different types of coatings, which are often based on various polymeric materials, have been developed to protect metal surfaces and inhibit the corrosion process [4,10]. Acrylic resins are considered the most suitable; thus, commercial products, such as the Paraloid family, have been extensively employed in the last three decades. Despite their proven advantages like the ease of application, good adhesion and mechanical properties, acrylic polymers show significant disadvantages, in particular, a lack of compatibility with copper and bronze surfaces, and degradation and yellowing after exposure to higher temperatures and sunlight [8].

Incralac is a commercial product based on ethyl methacrylate/butyl acrylate copolymer, with a composition devoted to acting as an anticorrosion treatment for copper artifacts. Basically, it is a solution of Paraloid B44, to which benzotriazole and epoxy soybean oil are added, and is extensively employed in the protection of copper artifacts. However, in the last decades, many drawbacks have been reported, in terms of changes in the color of metal surfaces after application, the relatively low protection performance when aged [11], and microorganism colonization, followed by biodegradation, which fosters the deterioration of protective films [12]. The major concerns are related to toxicity and the health risk to personnel involved in restoration procedures when using Incralac [13]. The modern approach in both industrial and cultural heritage coatings aims to develop more sustainable solutions, replacing traditional recipes with eco-friendly materials from renewable sources [14,15].

Fluoropolymers are also used as protective coatings, which are often combined with silanes in hybrid materials [16,17]. They possess important advantages, such as high photostability and resistance, in comparison with other polymers, but their applicability is hindered by low solubility in common solvents and reduced adhesion to metal surfaces. Filmogenic materials based on silane films have been proposed as coatings for a large variety of industrial applications, and have also been proposed for use in cultural heritage protection as a treatment for stone monuments and glass or paper artifacts, as well as for metal objects. For example, the silane derivative 3-mercapto-propyl-trimethoxy-silane (PropS-SH) was found to have significant anticorrosion efficiency on bare and aged bronze [18].

Silica coatings based on sol–gel materials with various organo-modified silane precursors have been studied, and superior superhydrophobic and resistance properties have been reported, with targeted applications being in industrial domains, with no esthetic limitations [19–21].

It is to be noted that for the cultural heritage domain, in most cases, silica coatings have been applied in the protection of stone monuments, where they exhibit high compatibility with lithic surfaces, and their lack of transparency does not change the appearance of the monuments [22,23].

As the interface between the material and the environment is the place where corrosion initiates, the surface morphology, texture and surface energy are key factors in controlling the corrosion behavior of metal samples. Coatings deposited on the metallic surface lead to

modification in the surface energy and hydrophobicity of the surface, with a significant effect on the corrosion resistance of the object [24].

Sol–gel-derived silica coatings, in particular, organic–inorganic hybrid ones, exhibit numerous advantages such as high anticorrosion protection, compatibility with a large variety of materials and tunable hydrophobic properties. However, their composition must be carefully adjusted in order to achieve the targeted optical properties, adherence and resistance of the deposited films onto cultural heritage objects [25,26].

There are some studies that report the synthesis and characterization of sol–gel silica materials as protective coatings for metals (bronze and brass), but the investigations do not contain a comparison with commercial products currently used in the restoration practice. Films prepared from 3-glycidoxypropyltrimethoxysilane (GPTMS) and methyltrimethoxysilane (MTMS) were prepared and deposited on copper and brass, and a visual inspection of the samples after exposure to high-sulfur/humidity conditions was evaluated, proving higher anticorrosion protection when the multilayer with fluoropolymer was deposited [27].

However, the majority of the reported coatings do not meet low toxicity, long life-service, compatibility with artifacts, transparency, reversibility, easy synthesis and low-cost properties, which are mandatory requirements for employment in cultural heritage [28–30].

As additives in protective coatings, some chemicals that act as corrosion inhibitors are employed, such as triazole derivatives. The best has been proven to be benzotriazole (BTA), which is very efficient on a score of metal artifacts, but especially on ancient coins [31]. However, the recent trend in cultural heritage research is the replacement of BTA due to its high toxicity and carcinogenic potential [32].

Various inorganic nanoparticles (NPs), in particular, metal oxides, have been investigated as less harmful anticorrosion agents. Among the tested nanomaterials, ZnO NPs have gained increased attention due to their facile synthesis, high UV shielding effect, compatibility with most film-forming materials and cost efficiency [33]. ZnO particles embedded in various coatings show good results in anticorrosion protection as applied on a variety of metallic surfaces [33].

Hydrophobic and anticorrosive materials prepared by mixing ZnO in a hybrid acrylic–silicone polymeric matrix have been prepared and tested on steel, with remarkable results in terms of surface hydrophobicity and anticorrosion protective efficiency [34].

We recently reported the preparation and characterization of some multifunctional coatings with hydrophobic and antibacterial coatings, based on Ag and ZnO NPs embedded in a fluoropolymeric matrix as a coating material for metallic objects of copper and steel [17]. The bilayer coatings were proven to have good adhesion, high anticorrosive efficiency and antibacterial effects against *Bacillus cereus*.

Based on our previous work, we here propose a novel, cost-effective and environmentally friendly coating based on hybrid ZnO NPs—a silica material as an anticorrosion protective treatment for copper cultural heritage artifacts. The transparent and resistant filmogenic matrix is prepared using a simple sol–gel method, from GPTMS and TEOS derivative, and its protective efficiency is compared to commercial Incralac products.

To the best of our knowledge, no hybrid silica coatings containing both ZnO NPs and azole derivatives as anticorrosion agents have been prepared. The influence of the presence of various concentrations of ZnO NPs in both silica and Incralac coatings is also studied. The composition of the novel silica nanocoatings is balanced in order to achieve simultaneous corrosion protective efficiency similar to the Incralac product in both reduced toxicity conditions and limited esthetic changes in the treated artistic objects.

2. Materials and Methods

2.1. Materials

For the silica coating materials, tetraethoxysilane (TEOS, 99%, Fluka, Philadelphia, PA, USA) and (3-glycidoxypropyl)trimethoxysilane (GPTMS, 97%, Alfa Aesar, Haverhill, MA, USA) were used as silane precursors. Solvents were methanol (MeOH, 99%, ChimReactiv SRL, Bucharest, Romania) and xylene (p.a., Adra Chim SRL, Bucharest, Romania), used

as received, without further purification. Hydrochloric acid (HCl, 37%) was purchased from Lachner, Neratovice, Czech Republic. Incralac lacquer (Incralac 44) and benzotriazole (BTA) were technical products for conservation purposes, purchased from CTS Europe (Florence, Italy).

For the synthesis of ZnO nanopowders, zinc nitrate hexahydrate ($Zn(NO_3)_2 \cdot 6H_2O$, purity > 98%, Aldrich reagent) and sodium hydroxide (NaOH) (purity $\geq$ 98%, Aldrich reagent) were purchased from Sigma-Aldrich (Merck Group, Darmstadt, Germany). Bidistilled water was produced by using a Milli-Q®Advantage A10 system (Merck Millipore, Darmstadt, Germany).

Copper foil (99.99%, thickness: ~5 mm) was used as the model metal to evaluate the anticorrosion efficiency, purchased from Tianjin Blueprints Iron & Steel Co. Ltd., Tianjin, China.

2.2. Methods

2.2.1. ZnO Nanoparticle Synthesis

For the preparation of ZnO NPs, a facile hydrothermal synthesis method adapted from the literature in our laboratory was used [35]. Briefly, a solution of 0.725 g $Zn(NO_3)_2 \cdot 6H_2O$ in 10 mL of bidistilled water was prepared and magnetically stirred at 40 °C. A second solution of 1 g NaOH dissolved in 7.5 mL H_2O was poured into the zinc precursor solution, and the mixture was kept for 30 min under magnetic stirring, while the aspect turned slightly opalescent. The reaction mixtures were transferred to a Teflon autoclave reaction vessel (Parr Instrument Co., Moline, IL, USA) and kept at 90 °C for 6 h. The solid powder was collected, separated by centrifugation and washed 5 times with distilled water to remove unreacted precursors. The freshly prepared ZnO nanopowder was dried at room temperature for 24 h and kept in dark for later use.

2.2.2. Nanocomposite Coatings Synthesis

The protective coatings were synthesized using a simple sol–gel method under acidic catalysis. A mixture of silane derivatives TEOS:GPTMS in a 2:1 molar ratio was dissolved in 10 mL of methanol. Then, aqueous hydrochloric acid 1M was added to start the silane precursor hydrolysis. The synthesis was performed under continuous magnetic stirring (750 rpm) at 25 °C for 1 h. No further thermic treatment was applied to the film-forming materials before the deposition on coupon samples. Coating materials were prepared with various contents of ZnO NPs (0.5%, 1%, 2% or 3% mass ratio according to silane precursor contents) and benzotriazole (0.15% and 0.3% mass ratio according to silane contents). The ZnO NPs and BTA were added to the reaction vials under magnetic stirring during the maturation of the silica gels. Some samples of silica-based coatings were prepared to contain both ZnO NPs and BTA. They were synthesized as described above for simple silica film. As a reference anticorrosion material, Incralac commercial product was used to produce protective films, using the recipe indicated by the producer (dilution of the commercial lacquer 5% in xylene). Incralac 44, also known as Incralac, was selected as reference material since it has been used in the conservation of metallic historic objects as anticorrosive treatment for many years and is still considered by the large majority of conservation practitioners as a valuable choice [13]. The commercially available product consists of Paraloid B44 (methyl methacrylate and ethyl acrylate copolymers) and benzotriazole in a mixture of organic solvents.

The ©ncralac solution containing various amounts of ZnO NPs was prepared by adding appropriate amounts of nanopowder and dispersing under magnetic stirring. After preparation, the nanocomposites were deposited on copper coupons by brushing, as this is the deposition method employed in conservation practice. The copper coupons were obtained by cutting the original copper foil, cleaned with commercial detergents and acetone and, finally, rinsed with alcohol. Before cleaning with solvents, the copper pieces were polished with commercial sandpaper in order to remove copper oxide and other residues from the metal surface. For AFM measurements, the films were prepared on microscope glass slides by sequentially dropping volumes of filmogenic materials. The

glass slides were previously washed with commercial detergents and rinsed with distilled water. The films were dried at room temperature for 24 h and then used for further characterization.

In Table 1 the composition of the coating materials is summarized.

Table 1. Composition of hybrid coatings.

Sample	Molar Ratio GPTMS-TEOS	ZnO (%)	Incral 44 Conc. (%)	BTA Conc. (%)
M1	–	–	5	Com. % [1]
M2	1:2	–	–	–
P1	–	0.27	5	Com. %
P2	–	0.5	5	Com. %
P3	–	1	5	Com. %
P4	–	2	5	Com. %
P5	–	3	5	Com. %
P6	1:2	0.5	–	–
P7	1:2	1	–	–
P8	1:2	2	–	–
P9	1:2	–	–	0.15
P10	1:2	–	–	0.3
P11	1:2	1	–	0.15
P12	1:2	0.5	–	0.3
P13	1:2	1	–	0.3
P14	1:2	2	–	0.3

[1] Com. %—concentration of BTA in the commercial product.

2.2.3. Characterization

Size and size distribution of the synthesized ZnO nanopowders were measured using dynamic light scattering (DLS) methods on a Zetasizer NanoZS instrument (Malvern Instruments Ltd., Malvern, UK). The selected samples were dispersed in bidistilled water at a concentration of 0.2 mg/mL and then subjected to ultrasonication for 10 min in an ultrasonic bath (Branson Ultrasonic Cleaner, Branson, Danbury, CT, USA).

X-ray diffraction (XRD) was performed using a Rigaku SmartLab instrument (Rigaku, Tokyo, Japan). The patterns were collected at room temperature using monochrome radiation Cu kα (λ = 1.5406 Å, 40 kV, 200 mA) and a scanning rate of 2 degrees per minute.

Reflectance spectra of the silica- and Incralac-based coatings were measured on a JASCO V-570 spectrophotometer (Jasco, Easton, MD, USA), in a range of 800 to 350 nm using Spectralon as standard. Colorimetric parameters (CIELab) were calculated using the software of the instrument.

Gloss analyses were performed using PCE-CM80 portable equipment (PCE Deutschland GmbH, Meschede, Deutschland), having a resolution of 1 GU, repeatability of 0.5% and accuracy of 1% (for measurements between 100 and 1000 GU), and a resolution of 0.1 GU, repeatability <0.45 GU, accuracy <1 GU (for measurements between 0 and 99.9 GU). For each sample, five measurements were performed, and the results are presented as means $\pm$ SEM. Statistical analysis of the results was conducted using freely available software [36]. Values are means $\pm$ SEM, n = 5 per treatment group. Means in a row without a common superscript letter differ ($p < 0.05$) as analyzed using one-way ANOVA and Tukey's test.

A contact angle Instrument, OCA 15 (DataPhysics, Filderstadt, Germany), was used for the evaluation of hydrophobicity of the surfaces, with water as a reference liquid. The static contact angles of water on deposited films were obtained using a sessile drop method at room temperature. The reported contact-angle values were obtained by analyzing the captured images, fitted with suitable equations provided by the instrument software. The reported contact angle main values were computed as the average of four–five measurements (liquid droplets placed in various regions of the film surface). Statistical analysis was

performed by using one-way analysis of variance (ANOVA) and *t*-test. A *p*-value < 0.05 was considered statistically significant.

Fourier-transform infrared (FT-IR) spectra were registered with a Bruker Vertex 70 instrument (Woodstock, NY, USA), equipped with a diamond crystal ATR accessory. The work conditions were 4 cm^{-1} resolution with 64 scans at 4000–400 cm^{-1}. Spectra were taken in triplicate, and highest-intensity spectra were kept for analysis.

The morphology of the prepared films was investigated using environmental scanning electron microscopy (ESEM). An FEI-Quanta 200 microscope (FEI, Eindhoven, the Netherlands) was employed, working under the following conditions: low vacuum, spot value of 2.5, variable magnification between 200 and 12,000×.

For the investigation of the composition of ZnO aggregates in films, X-ray energy dispersion spectrometry was performed. The samples were analyzed using an instrument consisting of a field-emission scanning electron microscope, Hitachi TM4000plus II (Hitachi, Hokkaido, Japan), coupled to a spectrometer by energy-dispersive X-ray (EDX). A BSE detector was used at an accelerating voltage of 15 kV with a magnitude of 200. The preparation of the samples for this study involved taking 40 μL of each suspension sample and depositing them on the carbon strip, drying them at room temperature for 24 h and then capturing SEM images and EDX spectra.

Atomic force microscopy (AFM) measurements were performed in non-contact mode with XE-100 (Park Systems, Suwon, Korea) in order to minimize the tip–sample interaction. All AFM images were recorded at scales of (8 × 8) μm^2 and (2 × 2) μm^2, with sharp tips, PPP-NCLR (Nanosensors^{TM}), with the following characteristics: less than 10 nm radius of curvature (typically 8 nm), 225 μm mean length, 38 μm mean width, ~48 N/m force constant and 190 kHz resonance frequency. AFM images were recorded at a scale of (2 × 2) μm^2 together with representative line scans (surface profiles). The topographical 2D AFM images were processed with the XEI program (v1.8.0, Park Systems) for tilt correction and roughness parameter evaluation.

The adhesion of deposited films was evaluated using tape test method, ASTM D3359, method B (cross-cut) [37]. Briefly, a specific pattern was scribed onto the coatings deposited on the copper substrates with a sharp blade. Then, scotch tape was applied on the surface, a moderate pressure was applied by hand in order to ensure full contact and, finally, was rapidly pulled off.

Electrochemical corrosion measurements were performed using a potentiostat–galvanostat system Autolab PGStat 12 controlled by General Purpose Electrochemical System (GPES) with Windows interface (version 4.9.007). Linear sweep voltammetry—Tafel plots were made in saline medium (3.5% NaCl solution) at room temperature. Three electrodes in one-compartment cell (10 mL) were used in all experiments: reference electrode was Ag/AgCl, counter electrode was platinum with large area and working electrodes were coated and bare copper plates. The scan rate was 10 mv/s, in a potential range of −0.8 to 0.4 V.

3. Results

3.1. Preparation and Characterization of ZnO NPs Used for the Hybrid Coating

ZnO NPs were prepared by using a facile hydrothermal synthesis previously reported [17], and the size distribution, morphology and crystallinity (Figure 1) were characterized.

The time and temperature of the maturation step in the ZnO NPs' synthesis play a crucial role in the size and crystallinity of the obtained nanopowder. At low temperatures (up to 60 °C), a mixture of Zn compounds with rather low crystallinity can usually be obtained, while high temperatures (in a range of 120–180 °C) lead to ZnO powders with superior quality, but they are energy-consuming [35]. Thus, an easy and cost-efficient method was used, with a medium time reaction performed at 90 °C in a Teflon autoclave vessel. Under the above-mentioned conditions, the solid product showed sharp signals in the XRD diffractogram, suggesting good crystallinity (Figure 1a). The XRD diffractogram contains peaks at 31.7°, 34.3°, 36.2°, 47.5°, 56.6°, 62.8°, 67.9° and 69.0° that correspond to the (100), (002), (101), (102), (110), (103), (112), and (201) crystal planes. The obtained XRD

patterns confirm the wurtzite hexagonal phase of ZnO NPs (JCPDS card number: 36-1451) and are similar to other reported data [35,38]. Moreover, Figure 1a shows no additional signals corresponding to impurities, confirming the high purity of our ZnO nanopowder.

(a)

(b)

(c)
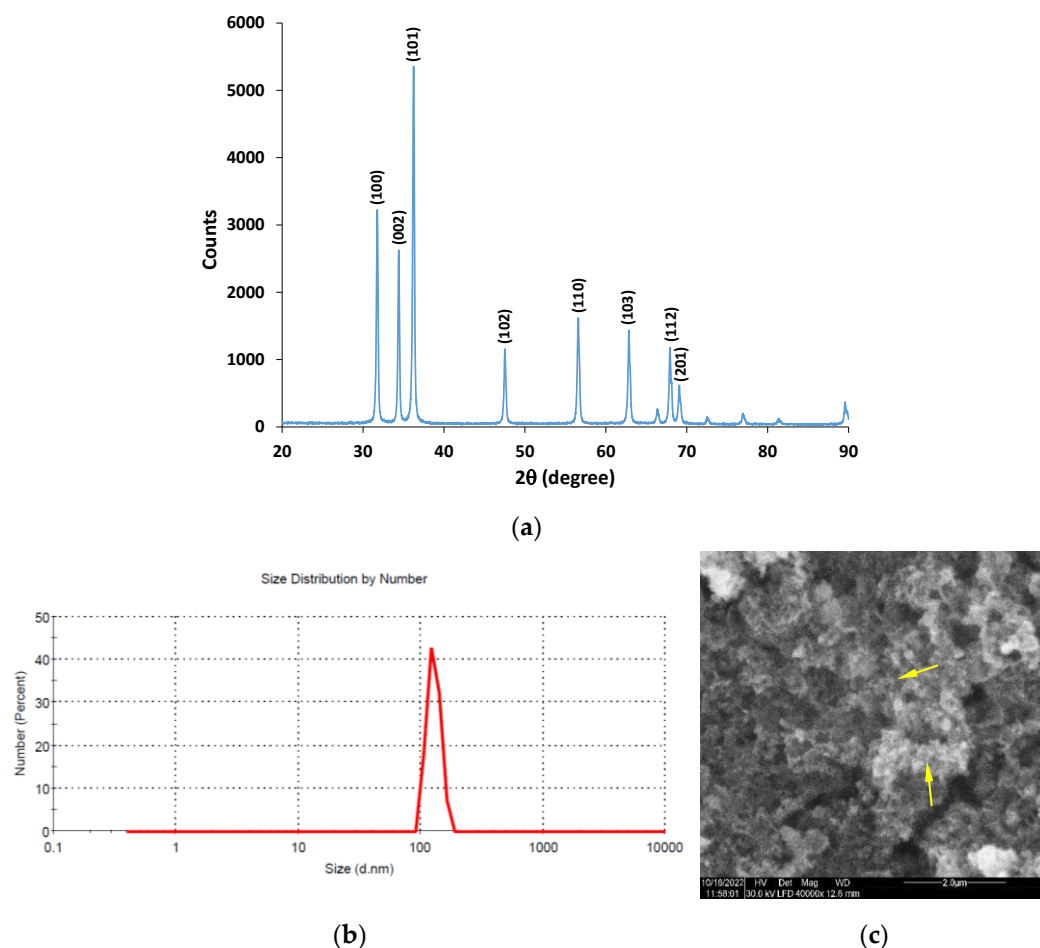
Figure 1. Physico-chemical characteristics of prepared ZnO NPs: (**a**) XRD diffractogram; (**b**) DLS diagram; (**c**) SEM image (the yellow arrows indicate ZnO nanoparticles).

The size of the crystallites was calculated according to Sherrer's equation using the line at 36.2° (the most intense), corresponding to the (101) plane. The average size of crystallites was found to be approximately 36 nm.

The DLS data prove that the produced ZnO NPs were monodisperse, with an average particle size of around 127.6 nm and a polydispersity index of 0.218 (Figure 1b). As compared to the size of the ZnO nanocrystallites obtained from XRD, it is presumable that the particles were polycrystalline. Figure 1c shows a representative SEM image of the particle morphology. It unveils quasi-spherical ZnO NPs, as expected, because no growth-regulating agent was used in the synthesis.

The as-prepared ZnO nanopowder was further dispersed in the film-forming materials without additional treatment.

3.2. Preparation of Organo-Modified Silica-Based Coating Materials

Various nanocomposite materials were prepared based on TEOS and organo-modified silane derivative GPTMS-TEOS, with ZnO NPs embedded and further deposited on copper samples (optical images in Figure 2 and Figure S1). In order to check the possible synergistic effects, various amounts of benzotriazole were added to the composition of the silane-based coating material.
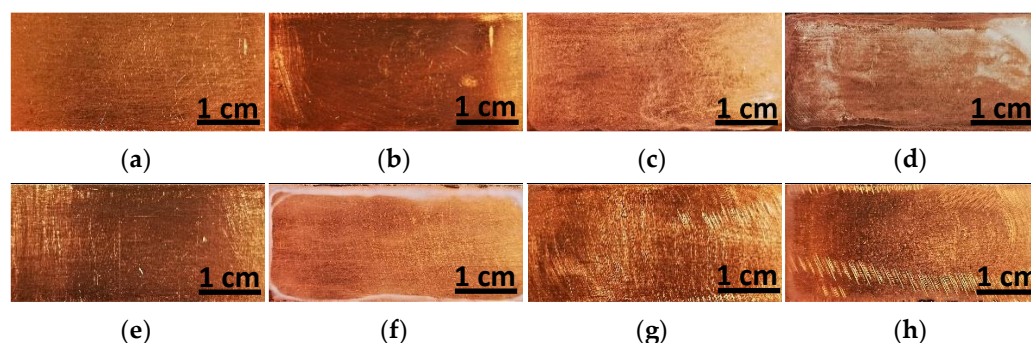
Figure 2. Representative optical images of Cu coupons coated with ZnO-silica nanomaterials and Incralac reference materials: (**a**) bare Cu; (**b**) Incralac (M1); (**c**) Incralac + 1% ZnO (P3); (**d**) Incralac + 3% ZnO (P5); (**e**) GPTMS-TEOS (M2); (**f**) GPTMS-TEOS + 2% ZnO (P8); (**g**) GPTMS-TEOS + 0.15% BTA (P9); (**h**) GPTMS-TEOS + 0.15% BTA + 1% ZnO (P11).

The images in Figure 2 show that the application of ZnO-silica nanomaterials did not significantly modify the color of the copper coupons.

Visual observations lead to the conclusion that the Incralac lacquer, as the reference coating material used in the conservation of cultural heritage objects, produced a thin, transparent, shiny film on the copper surface, as reported in the literature [13]. The addition of ZnO in concentrations up to 2% did not obviously change the appearance of the surface of the copper piece; instead, at concentrations of 3% ZnO, the appearance became slightly opaque due to the high content of NPs and their possible aggregation.

Figure 2 also contains pictures of Cu samples treated with the GlyTES-TEOS silane-based coatings. They show homogeneous films, with a slightly shiny look and without a change in the color of the metal. The addition of 2% ZnO NPs resulted in a less transparent film, while the presence of BTA up 0.15% had no effect on the visual aspect of the copper coupons. The simultaneous presence of BTA and ZnO NPs up to 1% produced a homogeneous transparent film.

### 3.3. Optical Characterization of Nanocomposite Films

Diffuse reflectance spectra were recorded and analyzed in order to evaluate the effect of the application of the ZnO-silica-based coatings, compared to Incralac-based ones, on the visual and esthetic aspects of the metallic coupons (Figures S1 and S2). The deposition of the Incralac lacquer resulted in a film with negligible effect on the absorption spectra recorded on the copper surface when compared to the bare metallic surface. The ZnO NPs added in concentrations up to 2% did not significantly change the spectra of the coatings, while a high content of ZnO material increased absorption in the region of 400–450 nm.

Minimal changes in the absorbance were also observed, as in the case of ZnO addition to the Incralac coatings at low nanoparticle concentrations compared to the pristine silica coating, but it is to be noted that this coating induced more changes in the visible spectra than the Incralac reference material. As expected, the presence of BTA did not produce any modification in the visible spectra of the silica coatings. Even for the silica-based nanomaterial samples that contained both BTA and ZnO NPs, smaller changes in the absorbance spectra could be observed compared to the material without additions.

The colorimetric parameters in the CIElab color space were determined from the diffuse reflectance spectra recorded in the domain of 380–800 nm. The chromatic coordinates *L**, *a** and *b** are defined as the brightness (ranging from 0 for black to 100 for white), the red–green component (considered + for red and − for green) and the yellow–blue component (+ for yellow and − for blue). The color modification is quantified using the equation:

$$\Delta E^* = \sqrt{\Delta L^{*2} + \Delta a^{*2} + \Delta b^{*2}} \tag{1}$$

The variation in the ΔE* values determined for coatings deposited on copper coupons is shown in Figure 3, and the chromatic coordinates *L**, *a** and *b** are listed in Table S1.
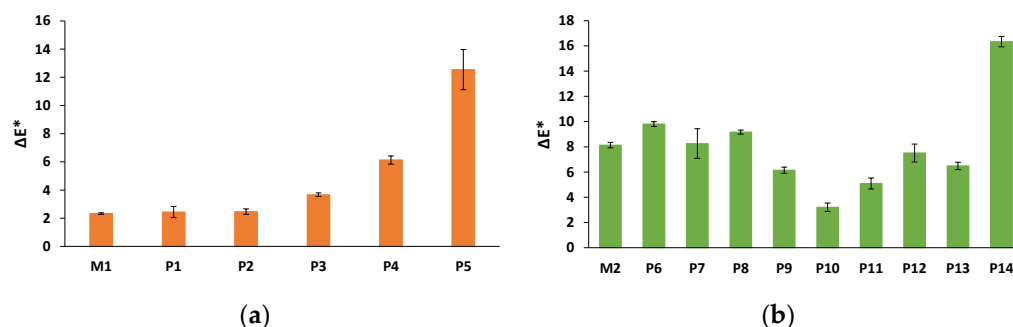
Figure 3. Variation in the total color difference (ΔE*) after deposition of coatings with various compositions: (**a**) Incralac-based coatings with various ZnO concentrations; (**b**) silica-based coatings with BTA and ZnO in various concentrations (compositions of coatings corresponds to Table 1).

A total color difference (ΔE) of less than 1 means the variation can be perceived only by experienced observers; between 2 and 3.5, an inexperienced observer can notice the difference; while between 3.5 and 5, a clear difference in color can be noted. For use in restoration practice, materials that produce a color difference, ΔE, of less than 3 or 5 are considered suitable [39,40]. However, in the recent literature, there are studies that question these limits by highlighting the influence of many factors such as the instrumentation quality, metamerism, illumination and the variance in the deposition method.

As shown in Figure 3, Incralac could be considered to produce minimal visual impact, with a color difference ΔE* of 2.22 ± 0.06, while the pristine silica coating is out of the acceptable range, with a statistically significant higher value ΔE* of 8.13 ± 0.22. The high values of color differences are mainly due to the defects of the silica films during the brushing procedure. The Incralac films with ZnO NP concentrations of less than 3% had all ΔE* < 5, while at high ZnO contents, a significant increase in the color difference occurred (Figure 3a). Regarding the silica-based coatings, the influence of ZnO NP presence showed similar behavior; little variations were induced compared to the pristine material at low concentrations of ZnO NPs. The presence of BTA together with ZnO NPs showed a beneficial effect: two of the coating samples with 0.15% and 0.30% BTA and 1% ZnO were close to the acceptance limit (Figure 3b).

The shiny aspect produced by the conservation products on ancient cultural objects, usually with the preserved original patina, is, in particular, a very sensitive issue in the decision of the material to be used in restoration procedures. Thus, the obtained coatings were investigated in terms of brightness using a glossmeter. The results are presented in Table 2, accompanied by the significance of the recorded differences obtained from one-way ANOVA and Tukey's tests.

Table 2. The gloss properties of the coatings.

Sample	Gloss (g.u.—Gloss Units)	Sample	Gloss (g.u.—Gloss Units)
M1	110 ± 4.96 [a]	P7	69.6 ± 6.02 [d,f]
M2	159 ± 1.66 [b]	P8	50.7 ± 5.55 [f,g]
P1	85.9 ± 6.03 [c,d]	P9	103 ± 2.71 [a,c]
P2	77.4 ± 4.67 [d]	P10	76.6 ± 4.02 [e,h]
P3	71.4 ± 0.653 [d]	P11	41 ± 5.02 [e,g]
P4	21.7 ± 0.664 [e]	P12	48.3 ± 2.83 [g]
P5	21.3 ± 0.707 [e]	P13	32.9 ± 2.91 [e,g]
P6	85.2 ± 5.66 [c,d]	P14	42.8 ± 2.01 [g,h]

For the Incralac lacquer (sample M1), it recorded high gloss values, as has often been reported in the literature [41].

However, in the restoration practice, the shiny aspect of the Incralac coatings is considered undesirable, in particular, for old works of art with original patina, and matting agents, such as waxes, are applied as the topcoats of anticorrosive treatments. The addition of ZnO NPs in the Incralac lacquer led to a decrease in glossiness, with a drastic reduction for contents in a range of 2%–3%. The pristine silica-based coating also produced a shiny surface of the deposited film, which was significantly reduced when ZnO NPs were added in concentrations of up to 2%. The presence of BTA together with ZnO NPs in the silica coatings led to the highest decrease in gloss values. As expected, the presence of ZnO NPs exhibits the main effect in the matting effect. Low concentrations of ZnO NPs (up to 1%) produced the same decrease in gloss for both the Incralac- and silica-based films. The decrease in gloss produced by the presence of high ZnO contents (2%–3%) in Incralac did not significantly differ from the effect produced by the high contents of ZnO together with BTA in the silica coatings.

3.4. FTIR Analysis

The composition of the hybrid coatings and the possible interactions between their components were investigated using FTIR spectroscopy. The FTIR spectra for some representative coatings containing ZnO NPs, BTA or both anticorrosion agents are presented in Figure 4.
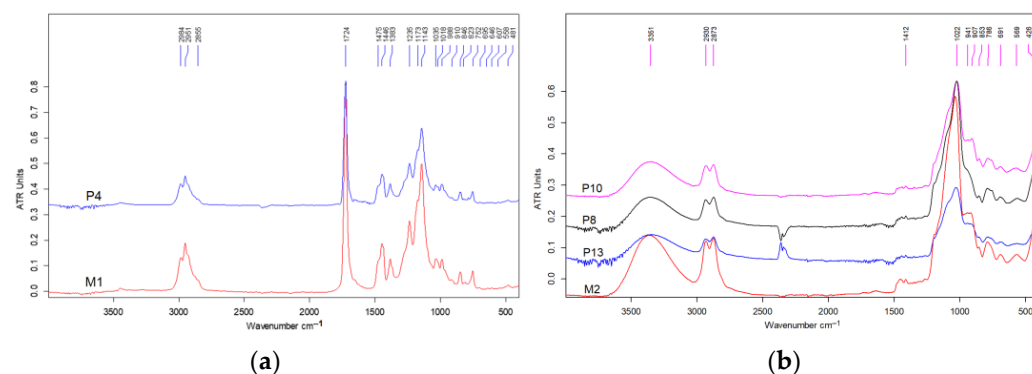
Figure 4. FTIR spectra for: (**a**) Incralac-based and (**b**) silica (GPTMS-TEOS)-based coatings, with various added BTA and ZnO NP concentrations.

Figure 4a reveals the signals of Paraloid 44, the main component of Incralac coating. They appear at 2985 cm^{-1} (C–H antisymmetric stretch, 2951 cm^{-1} (C–H symmetric stretch), 1724 cm^{-1} (C=O), 1447 cm^{-1} (CH$_3$–CH$_2$–O side chain), 1383 cm^{-1} (CH$_3$ side chain), 1236 cm^{-1}, 1143 cm^{-1} (C–O–C), 1035 cm^{-1} (C–C–O), 989 cm^{-1} (H–C–H, -CH$_3$), 847 cm^{-1} (C–C–CH$_3$). The O–H band can be identified at 3442 cm^{-1}. A very small concentration of benzotriazole can be detected by the presence of the specific band characteristic for the aromatic structure of BTA (aromatic ring C–H deformation vibration at 695 cm^{-1}). The spectra collected show similar peaks with the reported ones in the literature [42,43].

The Incralac-ZnO sample exhibits the typical Zn-O vibration at about 558 cm^{-1}. Also, small shifts in the band position and band intensity can also be observed, as compared to the Incralac coating without ZnO, which is due to the physical interactions between the ZnO surface and polymeric chains in the Incralac composition. This behavior is reported in the literature for ZnO NPs embedded in various polyacrylic polymeric matrices [44].

The silane-based nanocoatings show GPTMS and TEOS peaks, which are similar to the results reported in the literature [45].

The characteristic peaks are located at 3352 cm^{-1} (–OH band), 2931 cm^{-1} and 2873 cm^{-1} (C–H vibration), and the 1412 cm^{-1} C–H vibration of –CH$_2$ and –CH$_3$ groups. The signals at 1023 cm^{-1} correspond to the Si–O–Si bonds, 907 cm^{-1} (Si–OH) and small peaks at 786 and

692 cm^{-1} to Si–O–Si stretching vibrations. In the samples with complex composition, the ZnO peaks are present at about 570 cm^{-1}, while the BTA peak in the region of 690 cm^{-1} is absent due to the very small content of the azole derivative. Small shifts in the band position and intensity for the signals of the silane backbone can be observed for various compositions, suggesting a physical interaction between the ZnO NPs and the silica matrix components. No additional signals revealing the formation of new chemical bonds were recorded in samples with ZnO NPs or ZnO NPs and BTA, suggesting both anticorrosive agents do not chemically react with the filmogenic materials and could freely provide their anticorrosive action on the metallic surface.

3.5. Morphology of Nanocomposite Films

The morphology of the silica coatings with various additive components was evaluated from SEM images. For comparison, the Incralac lacquer with and without ZnO NPs was also investigated. In Figure 5, SEM micrographs are shown for the Incralac coatings, with various ZnO NPs concentrations.
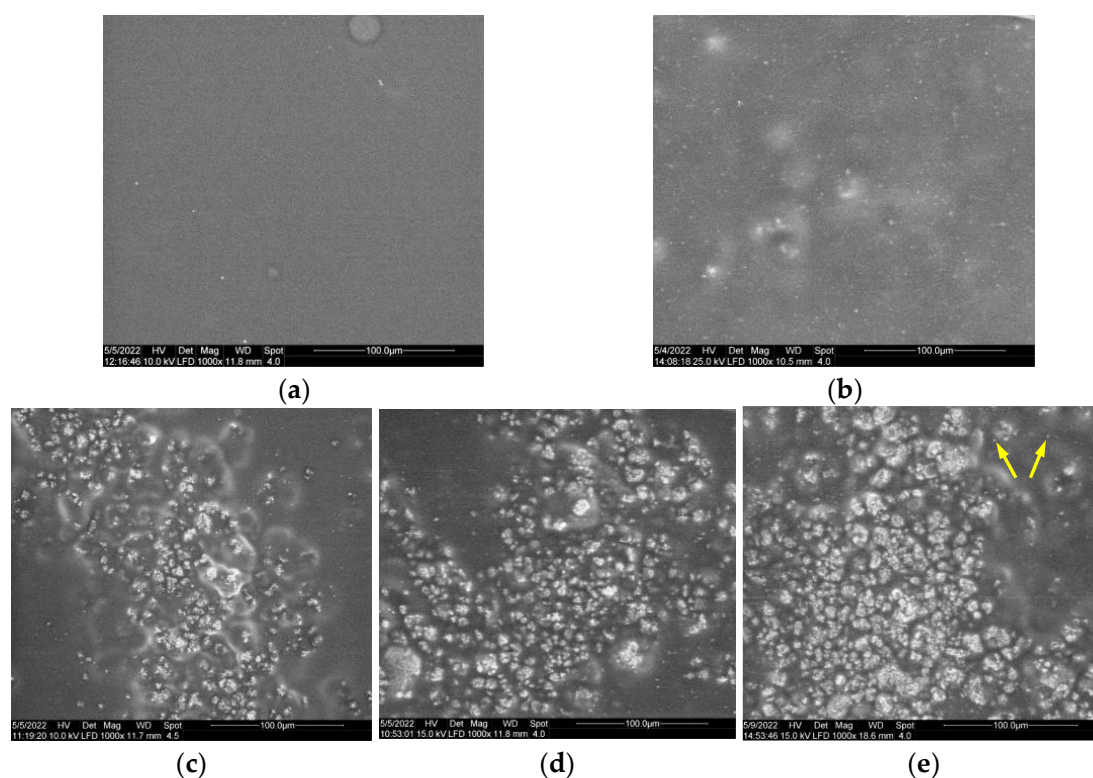

Figure 5. SEM images of Incralac coatings with various ZnO contents: (**a**) reference Incralac coating (M1 sample); (**b**) Incralac with 0.5% ZnO NPs (P2); (**c**) Incralac with 1% ZnO NPs (P3); (**d**) Incralac with 2% ZnO NPs (P4); (**e**) Incralac with 3% ZnO NPs (P5) (the yellow arrows indicate ZnO nanoparticles).

As previously reported [13], the commercial Incralac product formed uniform, smooth coatings. The addition of ZnO NPs to the Incralac lacquer prior to deposition resulted in the formation of rather large aggregates due to the low dispersibility of the ZnO nanopowder in the nonpolar solvent of the coating material (Figure 5b–d). The increase in the ZnO concentration, up to 3%, further increased the size of the particle aggregates, and the coating aspect became less homogeneous (Figure 5e).

Figure 6 shows representative images for the GPTMS-TEOS silica coatings, containing various amounts of ZnO NPs and BTA.

The addition of ZnO NPs into the silica material after the polymerization of silane derivatives produced a very homogeneous coating, with no morphologically significant differences to the pristine GlyTMES-TEOS silica film (Figure 6a,b). This is possible due

to the better dispersion of the hydrophilic ZnO NPs into the alcoholic solvent of the silica matrix. When the anticorrosion reagent BTA was introduced into the formulation of silica coating, no significant changes in the micrographs of the deposited films could be observed (Figure 6c,d). The simultaneous presence of the ZnO NPs and BTA led to the aggregation of the ZnO NPs (Figure 6e) but to a significantly lower extent compared to a similar composition in the Incralac lacquer (Figure 5c).
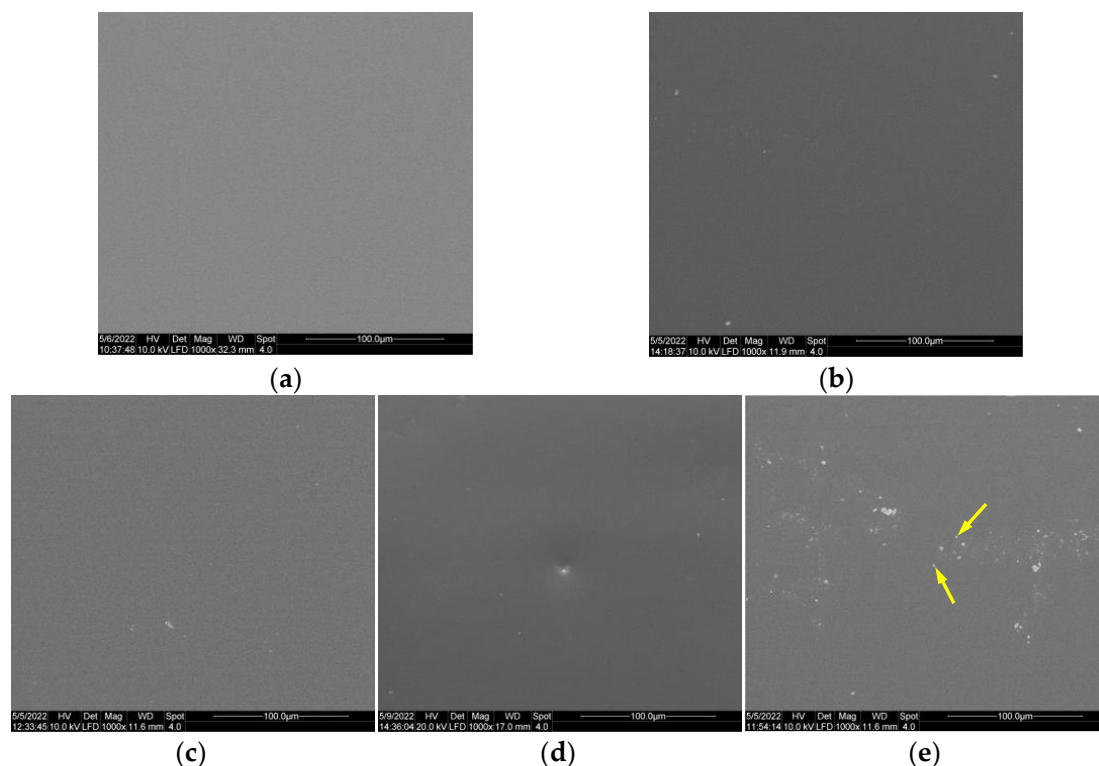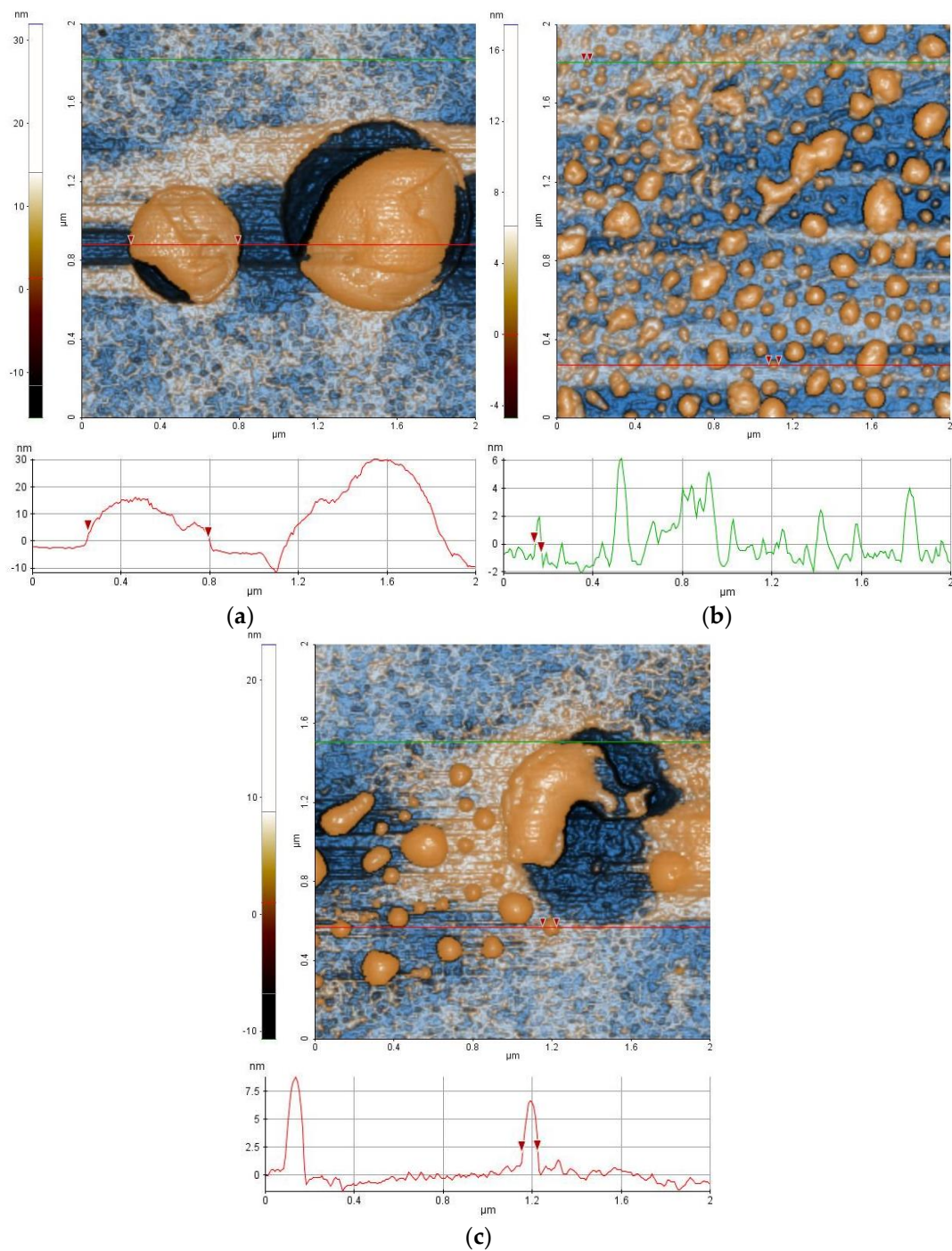

Figure 6. SEM images of silica coatings with various ZnO NP and BTA contents: (**a**) reference GPTMS-TEOS silica coating (M2 sample); (**b**) silica coating with 1% ZnO NPs (P7); (**c**) silica coating with 0.15% BTA (P9); (**d**) silica coating with 0.3% BTA (P10); (**e**) silica coating with 1% ZnO NPs and 0.15% BTA (P11) (the yellow arrows indicate ZnO nanoparticles).

The elemental composition of the aggregates observed in the Incralac-based and silica-based films (Figures 5c–e and 6d,e) was investigated by using energy-dispersive spectrometry. The EDX plots and corresponding SEM images are presented in the Supplementary Materials (Figure S3).

The EDX plot for the ZnO aggregate in the Incralac film (Figure S3b) shows the peaks for Zn and O, with an additional signal for C due to the carbon strip used as the sample stab. In the case of smaller ZnO aggregates in the silica-based film (Figure S3c), the major signals are for Zn and O, confirming the composition of the aggregate, while the other signals (Si, for example) appear due to the presence of the silica material, in which ZnO was embedded.

AFM was the next step in the morphological characterization of the nanocomposite films. The tests were carried out to observe whether the presence of ZnO and BTA changes the topography of the base films deposited on microscope slides. The AFM images are presented in an "enhanced color"™ view in order to highlight the morphological features. Representative line scans were selected to show the z-scale (surface profiles) on a nanometric range (z-scale). Enhanced-contrast bi-dimensional (2D) AFM images of Incralac and GPTMS—TEOS are shown in Figures 7 and 8.

Figure 7. Topographic images of Incralac coatings with various ZnO NP contents: (**a**) reference Incralac coating (M1 sample); (**b**) Incralac coating with 0.5% ZnO (P2); (**c**) Incralac coating with 1% ZnO (P3).

The coating deposited from pristine silica shows a very smooth surface, confirming the homogeneous morphology observable in the SEM images. On the contrary, for the reference Incralac coating, some large entities appear, which are probably due to the drying defects of the polymeric material on the hydrophilic surface of the glass (Figure 7a). The Incralac films containing ZnO NPs exhibit a large amount of aggregates, with various sizes and irregular shapes (Figure 7b). Those aggregates become larger as the concentration of ZnO increases (Figure 7c), a result that agrees with the inhomogeneous aspect in the SEM micrographs.
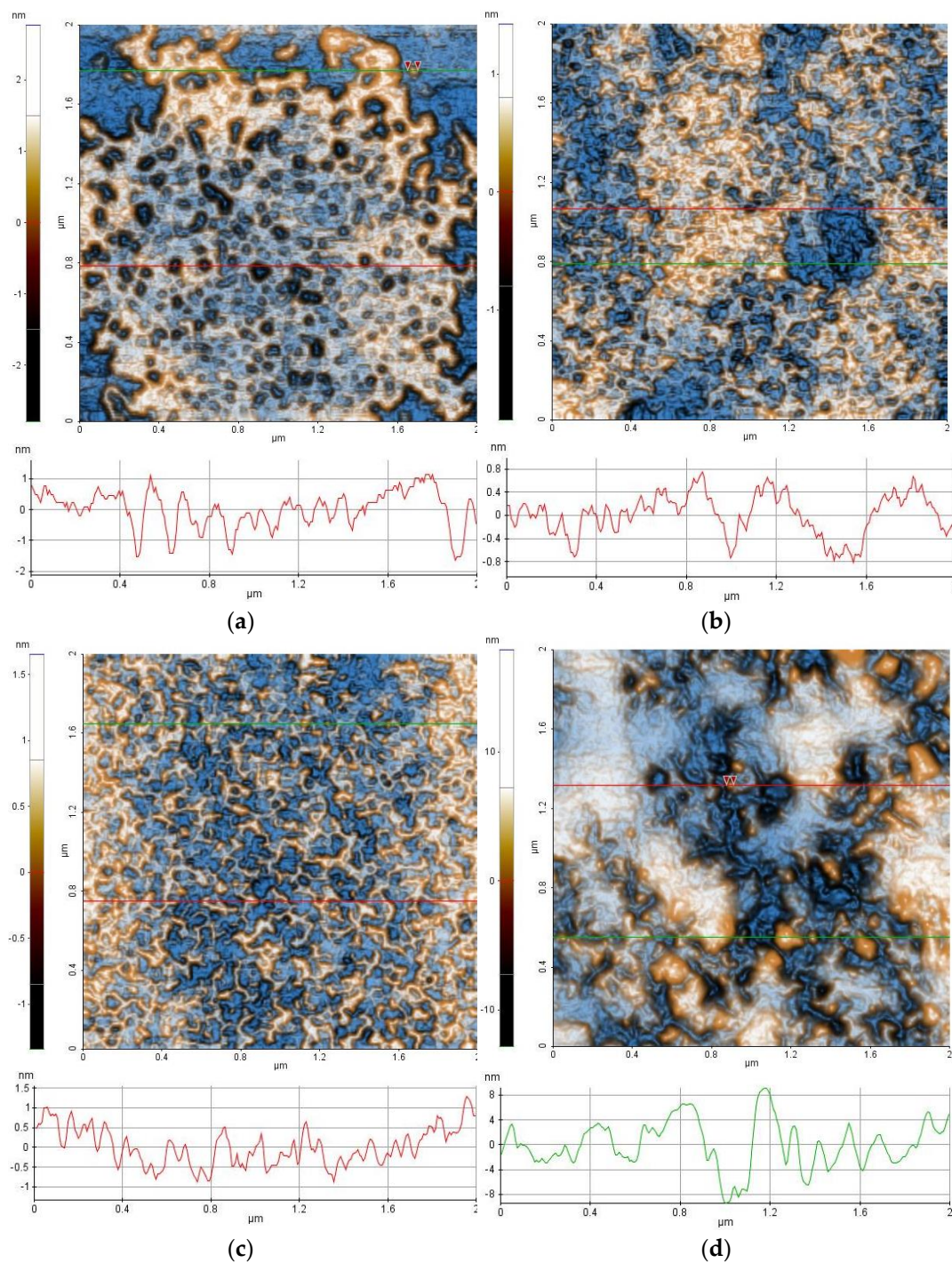
Figure 8. Topographic images of silane GPTMS-TEOS coatings with various BTA and ZnO NP contents: (**a**) pristine silica coating (M2 sample); (**b**) silica coating with 1% ZnO (P7); (**c**) silica coating with 0.15% BTA (P9); (**d**) silica coating with 1% ZnO NPs and 0.15% BTA (P11 sample).

The separate addition of BTA and ZnO NPs did not change the topographical appearance of the coating produced from silica-based materials (Figure 8b,c). When both adding agents are present, even in small amounts, a tendency of aggregation occurs and ZnO larger aggregates are visible.

The root-mean-squared roughness (Rq) represents the standard deviation of the height value in the image; the average roughness (Ra) is the average deviation from the mean height, the area between the roughness profile and its mean value per unit length; while the peak-to-valley parameter (Rpv) of the image or line is the height difference between

the lowest and the highest points in the analyzed area. Figure 9 illustrates the roughness variation for both the Incaralac and silane-based films.
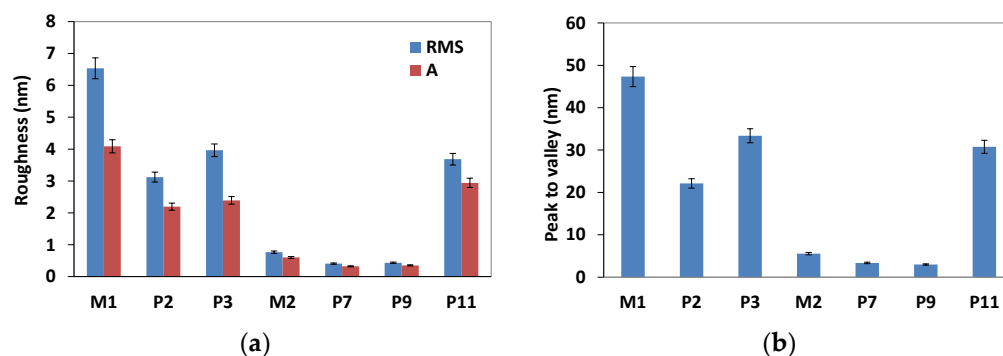
Figure 9. The roughness variation with the composition of the Incralac (**a**) and silica-based coatings (**b**).

Coatings obtained from the pristine silica GPTMS-TEOS material (M2) and the ones with ZnO NPs 1% and with BTA (P7 and P9) are characterized by low corrugation parameters (RMS (Rq) and average (Ra) roughness) of less than 1 nm (Figure 9a,b). This is also reflected in the z-scale profiles (line scans collected along horizontal scan direction), as plotted in Figure 8 (the corresponding AFM images), of only 1–3 nm, as well as from the values of the peak-to-valley (Rpv) parameters of less than 6 nm. The simultaneous presence of ZnO NPs at 1% concentration and BTA leads to higher values in the roughness and peak-to-valley parameters (for example, sample P11, characterized by a succession of hills and valleys).

For coatings produced from pristine and modified Incralac lacquers, unexpectedly high values of the roughness and peak-to-valley parameters are due to the appearance of the agglomeration of materials in the form of protruding hemispherical particles of 50–200 nm (sample P2) or hundreds of nm, in the case of sample P3. The pristine Incralac coating also exhibits rare, large agglomerates. This leads to RMS values in the range of 4–7 nm and peak-to-valley parameters in the range of 22–47 nm.

The values of the determined roughness confirm the conclusions of the SEM micrographs and topographic AFM images. However, even in the samples in which inhomogeneities appear on the nanometric scale, the roughness is still at a low level and, in most cases, does not significantly influence the macroscopic visual aspects. The influence of ZnO aggregation is more obvious in the non-polar solvent of the Incralac product, and is expected to lead to higher modifications in the resistance and adhesion of the films. The variation in the roughness of the modified coatings will be further discussed in correlation with the corrosion data, as this parameter is known to significantly influence the pitting susceptibility and corrosion rate of metals and alloys, such as copper, magnesium alloys and stainless steel [46].

3.6. Wettability and Adhesion of the Coating Materials

The wettability properties of the coatings were evaluated by using the determination of water contact angles on the coated surfaces. The results are presented in Figure 10.

As shown in Figure 10, both reference films made from Incralac and GPTMS-TEOS silica are hydrophilic in nature, with average CA values of the coatings of $73.4 \pm 1.32°$ in the case of Incralac and a significantly higher value ($p < 0.05$), close to 90° ($90.35 \pm 4.97°$), for the pristine GPTMS-TEOS silica film. The hydrophilicity of the commercial Incralac coating is consistent with its composition. The addition of the hydrophilic ZnO NPs in high concentrations, up to 3%, does not influence the contact angle values (Figure 9a). Unexpectedly, for samples containing low amounts of ZnO NPs (0.5%), the contents of added particles, together with the presence of larger aggregates on the surface, lead to a statistically significant increase in the contact angle value compared to the Incralac coating without the ZnO nanopowder.
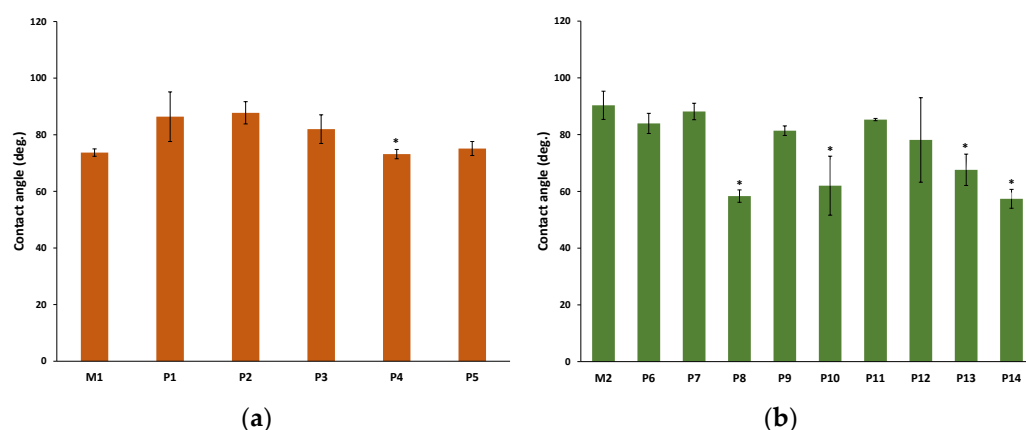
Figure 10. Contact angle values of Incralac coatings (**a**) and silica-based coatings (**b**) with various compositions; * means $p < 0.05$.

The organo-modified silica coating shows a contact angle in the range of the reported values from other coatings, depending on the molar values of the silane precursors [47]. For silica-based coatings with low contents of ZnO NPs, up to 1%, no variation in the wettability is evidenced, while an addition of 2% ZnO NPs produces a significant decrease ($p < 0.005$), and a determined value of $58.33 \pm 2.18°$. The addition of the anticorrosion reagent, BTA, at low concentrations, does not change the contact angle value of the GPTMS-TEOS film. At higher concentrations of BTA, the hydrophilic nature of the anticorrosion supplement leads to a moderate decrease in hydrophobicity.

Similar behavior can be observed for silica films when high concentrations of BTA are simultaneously present with rather high concentrations of ZnO NPs, for which the recorded contact angles exhibit average values of $67.6 \pm 5.53°$ and $57.38 \pm 3.33°$, respectively. The GPTMS-TEOS coatings with low contents of BTA together with a high amount of ZnO NPs or high BTA contents together with low concentrations of 0.5% ZnO NPs exhibit contact angles similar to those of the pristine silica film (average values of $83.6 \pm 0.4°$ and $78.13 \pm 14.88°$, respectively).

The prepared ZnO-silica nanocomposites show contact angles that suggest low hydrophobicity, with a tendency to become more hydrophilic when adding high concentrations of solid nanopowder and/or BTA. A superior hydrophobic property of the coating material would represent an advantage in increasing the anticorrosive effect by reducing the contact between the water and the covered metallic surface. Some strategies usually focus on increasing the hydrophobicity of silica filmogenic materials; unfortunately, these have not been reported to be successful in the development of coatings suitable for the cultural heritage field [48]. It is to be noted that these reported coatings show significant roughness and inhomogeneous aspects, as revealed by SEM images, while no study was performed to evidence the esthetic changes produced by the application on the metal surfaces. Thus, it is unlikely that such superhydrophobic coatings are suitable for restoration purposes. Other hydrophobic coatings for the protection of bronze and copper metallic objects have recently been reported, using the fluoropolymer resin, Lumiflon, crosslinked with poly(isocyanate). According to the chemical composition of the resin, the contact angles range from 78.6 to 112°, which is low compared to the expected values for fluoropolymers [49]. Even if the presence of fluorinated derivatives usually leads to an increase in the hydrophobicity of the coating, the toxicity and high price of these materials make them undesirable in the current practice of restoring cultural heritage objects, especially large ones.

Thus, it can be considered that the solution we propose in this study leads to obtaining coating materials with a significantly higher hydrophobicity than the commercial Incralac product, and which, although it does not have superhydrophobic properties, has multiple advantages in terms of minimal changes in the appearance of objects and ensures the increased reversibility of the treatment.

All the obtained silica coatings were characterized in terms of adhesion on the metal mock-ups using a tape test. For each copper plate sample, specific patterns with vertical and horizontal incisions were made; then, the scotch tape was applied, pressed and plucked. Representative optical images of some coatings subjected to the ASTM D3359 [50] adhesive strength test are presented in Figure 11.
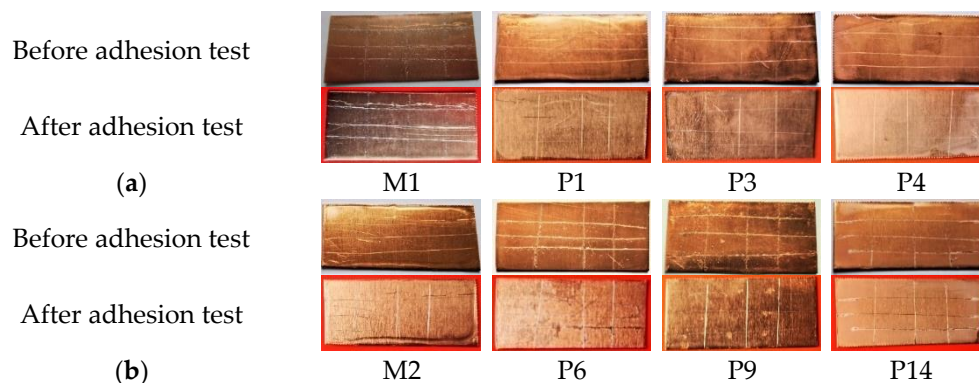
Figure 11. The optical images of coatings subjected to the test tape adhesion test: (**a**) Incralac-based coatings with various concentrations of ZnO NPs (codification samples as in Table 1); (**b**) silica-based coatings with various concentrations of BTA and ZnO NPs (codification samples as in Table 1).

The adhesion property was ranked on a scale according to Standard AAA, from 5B (no detachment, which is considered good adhesion) up to 1B (poor adhesion); the sample exhibited more than 65% detachment. The obtained results are presented in Table 3.

Table 3. Silica and Incralac-based coating adhesion.

Sample	Adhesion	Sample	Adhesion
M1	4B	P7	4B-3B
M2	4B	P8	4B-3B
P1	4B-3B	P9	3B
P2	4B-3B	P10	3B
P3	3B	P11	2B-3B
P4	3B	P12	2B-3B
P5	2B-3B	P13	2B
P6	4B-3B	P14	2B

For both pristine coatings (M1 and M2 samples), good adhesion properties were shown since neither exfoliation nor significant marks on the scotch tape after pulling off could be observed. A low detachment percentage was noticed for the Incralac coatings with ZnO concentrations up to 0.5%; consequently, the adhesion was very close to the reference coating. As expected, the loading of hydrophilic ZnO NPs, at high concentrations, into a rather hydrophobic coating material, such as Incralac lacquer, decreased the adhesion of the film on the metal surface. The Incralac films with 1%–3% ZnO NPs showed exfoliation on the edge of samples, together with a tendency to remove the upper layer of the coating, attached to the scotch tape when this was pulled off. The same effect of decreasing the adhesion on the copper substrate was observed when ZnO NPs were embedded in the silica-based materials.

Previous studies reported that coatings with the same compositions as Incralac, but without BTA, exhibited a higher degree of adhesivity on metals [51]; thus, we expected a similar effect with silica-based coatings containing benzotriazole. On the contrary, for our organo-modified silica coating, the presence of BTA led to a decrease in the adhesion of the films at both tested concentrations. A further decrease was observed for coatings containing ZnO NPs and BTA in various ratios, with the lowest adhesion being registered in the case of high BTA contents and 1% ZnO NP concentrations. However, it is to be noticed that similar

values for the adhesion test were reported in survey studies on commercially available Incralac-based coatings from various producers [51], with adhesion properties ranked from 5B to 2B. In conclusion, it seems that the addition of ZnO NPs, despite its targeted beneficial effect on anticorrosive protection, leads to a decrease in the adhesion and resistance of the coating. Thus, such ZnO-polymer nanocomposites are not particularly suitable for the long-term conservation of metallic artifacts. On the other hand, these coatings could be a valuable alternative for the temporary protection of archaeological objects immediately after excavation.

3.7. The Anticorrosion Efficiency

Linear sweep voltammetry (LSV) is one of the most used techniques to evaluate the corrosion process. It involves sweeping the potential applied at a working electrode and measuring the current response. With LSV, one can obtain important information concerning the susceptibility of materials to corrosion, the mechanisms of corrosion and the rate of corrosion.

Figure 12 shows images of copper samples coated with different materials before and after the corrosion measurements.
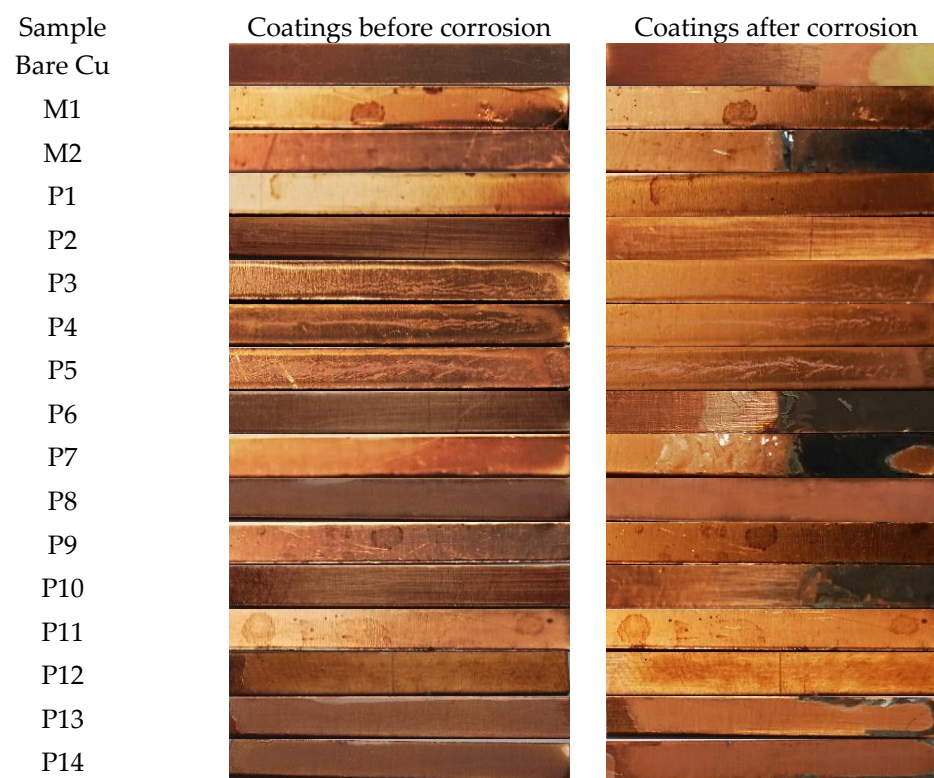
Figure 12. Images of Cu coupons coated with Incralac and with silica-based materials before and after the corrosion measurements. Right side of the copper bare was immersed in a 3.5% NaCl solution during the electrochemical determinations.

The presence of corrosion products is clearly observable for the samples coated with Incralac and silica materials without additional components. The effect is more pronounced for the silica film. In the case of P6, P7 and P10 specimens coated with modified silica materials, such as samples P6, P7 and P10, the content of corrosion products seems also to be high.

The Tafel polarization curves of the bare and coated copper plates were obtained after their exposure to the saline solution (NaCl 3.5%). The results are presented in Figure 13 for the different types of coatings.
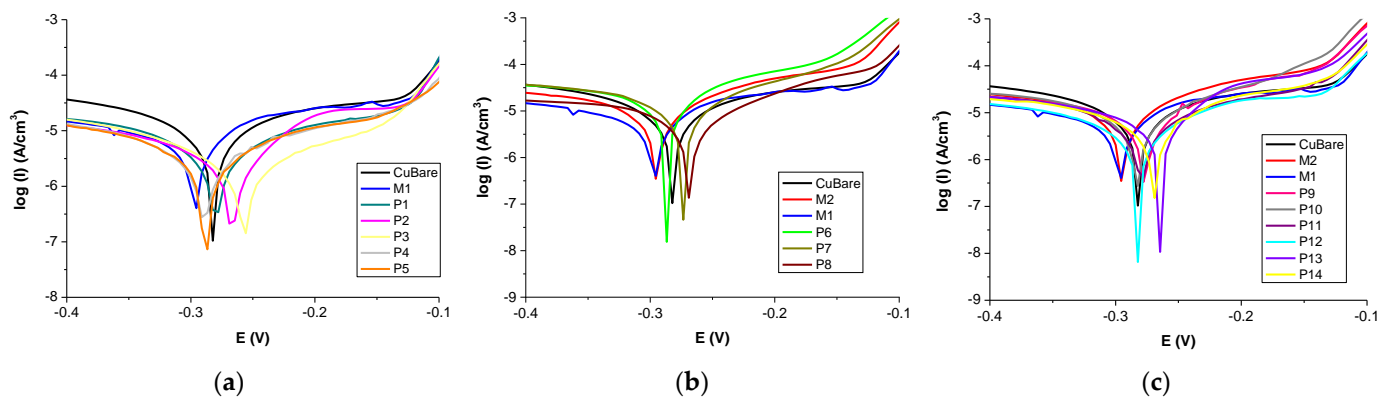
Figure 13. Tafel polarization curves determined for copper coupons coated with Incralac and silica-based materials with various compositions: (**a**) Incralac with various ZnO concentration; (**b**) silica-based with various ZnO concentration; (**c**) silica-based with various ZnO and BTA concentration (samples codes in Table 1).

The corrosion parameters including the polarization resistance (R_p), corrosion potential (E_{corr}), corrosion current density (I_{corr}) and corrosion rate are given in Table S2 (Supplementary materials).

The variation in the corrosion rate was computed, and the results are presented in Figure 14 as a function of coating composition.
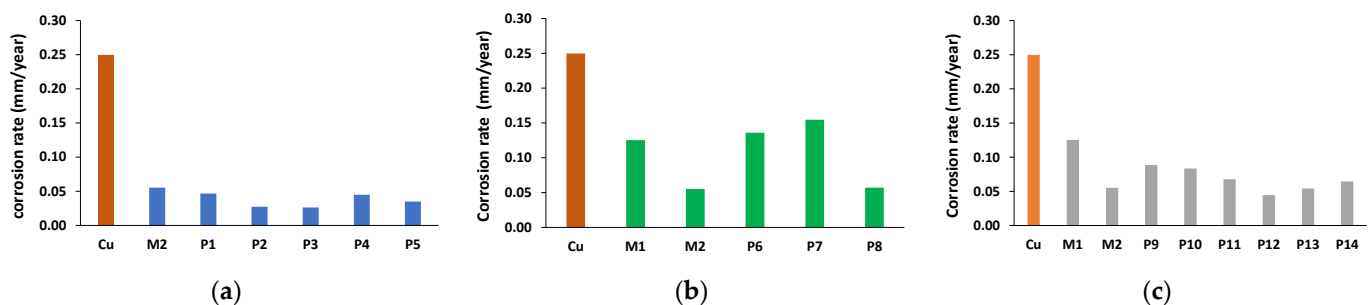
Figure 14. Variation in the corrosion rate for Incralac coatings with various contents of ZnO NPs (**a**); for silica GPTMS-TEOS films with various concentrations of ZnO NPs (**b**); and for silica GPTMS-TEOS films with the composition complex of ZnO NPs and BTA (**c**).

Compared to the bare Cu coupons, which had a rate of corrosion of approximately 0.25 mm/year, the Incralac coating reduced the value to 0.055 mm/year, while the unmodified silica coating was less effective, with a corrosion rate of 0.125 mm/year.

The addition of ZnO nanopowders to Incralac materials led to an expected decrease in the corrosion rate, with the lowest values for medium concentrations of ZnO NPs (0.027 mm/year for 0.5% and 0.026 mm/year for 1%). When the ZnO NP contents were 2%–3%, the corrosion rate increased up to values comparable to those of the pristine Incralac material.

For silica-based materials, the addition of ZnO NPs, up to 1%, did not influence the anticorrosion effect, while a reduction in the corrosion rate was observed only for 2% ZnO, where a value of 0.057 mm/year was measured, which is similar to the one recorded for the reference Incralac coating.

Beyond the intrinsic anticorrosion effect of the ZnO nanopowder in the composition of the coatings, the influence of the morphology and roughness must be taken into account. The microstructure of the coatings influences anticorrosion efficiency in many ways, changing the mechanical resistance and adherence of the film, increasing the surface exposed to corrosive factors, generating spots for localized corrosion and modifying the hydrophobic properties of the surface [52,53].

It is expected that physical interactions between ZnO NPs and the Incralac or silica matrix decrease the coherence of the deposited film, and this effect is more intense when ZnO concentration is higher and large aggregates are formed. This explains the higher corrosion rate recorded for Incralac lacquer containing a high concentration of ZnO NPs (3%) compared to coatings with 1% content when the values of roughness and the peak-to-valley index confirm the formation of large ZnO aggregates, which is also observable in the SEM images. The effect of the variation in ZnO NP contents in silica-based coatings is less obvious, as the modification in the roughness produced is smaller, due to the lower aggregation tendency of ZnO particles in the alcoholic solvent.

Since both coating matrices, Incralac and GPTMS-TEOS silica, are hydrophilic in nature, the increase in the surface roughness did not increase the contact angle value, as in the case of hydrophobic surfaces. The micro/nano-structure of the coatings containing various amounts of ZnO NPs tends to decrease the contact angle value, together with the increase in hydrophilicity produced by the presence of the ZnO component. Moreover, one can consider that in samples with higher contents of ZnO NPs, which show an increased tendency for aggregation and, consequently, surfaces with higher roughness, the anticorrosive protection is expected to be lower than in the case of more homogeneous, smooth coatings, with a uniform dispersion of unaggregated ZnO NPs.

As expected, the addition of BTA in the composition of the GPTMS-TEOS filmogenic materials led to an increase in the protective efficiency of the coating. However, in a range of 3 mg and 6 mg BTA contents, the values of corrosion rates are very similar (0.089 mm/year and 0.83 mm/year, respectively).

A further decrease in corrosion was recorded for copper coupons coated with silica-based materials, with both ZnO NPs and BTA in the composition. The best performances for anticorrosion effect were obtained for samples with high contents of BTA and moderate concentrations of ZnO NPs (below 2%), with values of corrosion rate comparable to the Incralac lacquer. A lower effect was observed when increasing the ZnO content up to 2%, probably due to the aggregation tendency that occurs in this case.

4. Conclusions

Hybrid silica materials, based on GPTMS and TEOS precursors, with loaded ZnO NPs were successfully prepared using a simple sol–gel method under mild conditions. The filmogenic materials were designed to fit the specific requirements of cultural heritage as protective coatings for the conservation of historic objects or monuments made of copper. The silica matrix and additional components have a low impact on the environment and low health risks for restoration practitioners. In addition, they have similar anticorrosion efficiencies to the reference material, Incralac, currently used in restoration works.

The physico-chemical and morphological characterization of the GPTMS—TEOS silica coatings, with various contents of ZnO NPs and BTA, were performed, and the results were compared to the reference coating from commercial Incralac. The addition of ZnO NPs, in both silica-based and Incralac-based coatings, led to minimal to moderate changes in the visual aspect and optical properties of the film-treated copper coupons, depending on the concentrations of nanopowder. At high concentrations of ZnO, an aggregation tendency was noticed, as proven by the SEM and AFM images. However, highly homogeneous coatings, even at the nanometric scale, were obtained for GPTMS—TEOS silica coatings with ZnO concentrations up to 1% and low BTA contents, which were similar to the pristine silica films. Electrochemical measurements were performed to evaluate the anticorrosive protection of the deposited films on copper solid substrates, emphasizing the effect of ZnO NP and BTA presence in both Incralac-based and silica-based materials.

Among the samples described in this work, the two GPTMS—TEOS silica coatings containing both ZnO NPs and BTA are suitable substitutes for the reference Incralac product used in the conservation of copper artifacts. The reasons for recommending them for such purposes are (i) better anticorrosion efficiency and adhesion to copper surfaces; (ii) films with high homogeneity, visual aspect and optical properties; (iii) the lack of harmful

organic solvents; and (iv) reversibility and ease of fabrication. The adhesion to the metal surface of the prepared silica coatings was in the range of the behavior reported for various commercial Incralac coatings. Thus, the GPTMS—TEOS silica coatings containing rather low amounts of ZnO NPs and BTA seem to be a possible replacement for Incralac products in the protection of copper archaeological artifacts, at least for temporary conservation, in the period between excavation and final restoration and exposure in a museum.

Although the anticorrosion protection performance of the proposed protective material was not significantly improved compared to the currently used Incralac lacquer, the advantages of the new nanohybrid coating are obvious in terms of the elimination of toxic solvents and the use of low concentrations of anticorrosion components while keeping within acceptable limits the impact on the appearance esthetic of the artistic object subjected to treatment.

Further studies are required to evidence the preservation of the efficiency and optical properties of the proposed coatings after long-term applications on outdoor monuments.

Since the best results were recorded for silica-based materials with both ZnO NPs and BTA, further systematic studies need to be conducted to allow for evidence of the interaction between the two anticorrosive components and the quantification of possible synergistic effects.

References

1. Watkinson, D. Conservation, Corrosion Science and Evidence-Based Preservation Strategies for Metallic Heritage Artefacts. In *Corrosion and Conservation of Cultural Heritage Metallic Artefacts*; Elsevier: Amsterdam, The Netherlands, 2013; pp. 9–36, ISBN 978-1-78242-154-2.
2. FitzGerald, K.P.; Nairn, J.; Skennerton, G.; Atrens, A. Atmospheric Corrosion of Copper and the Colour, Structure and Composition of Natural Patinas on Copper. *Corros. Sci.* **2006**, *48*, 2480–2509. [CrossRef]
3. Sørensen, P.A.; Kiil, S.; Dam-Johansen, K.; Weinell, C.E. Anticorrosive Coatings: A Review. *J. Coat. Technol. Res.* **2009**, *6*, 135–176. [CrossRef]
4. Cui, G.; Bi, Z.; Wang, S.; Liu, J.; Xing, X.; Li, Z.; Wang, B. A Comprehensive Review on Smart Anti-Corrosive Coatings. *Prog. Org. Coat.* **2020**, *148*, 105821. [CrossRef]

5. Zhou, D.; Chen, Y.-X.; Yuan, X.-Y.; Chai, Z.-L.; Liu, J.-K. Gradient Design of Vacancies and Their Positive Correlation with Electrochemical Anticorrosion Protection. *Inorg. Chem.* **2022**, *61*, 8053–8065. [CrossRef]

6. Wang, J.; Du, M.; Li, G.; Shi, P. Research Progress on Microbiological Inhibition of Corrosion: A Review. *J. Clean. Prod.* **2022**, *373*, 133658. [CrossRef]

7. Langroudi, A.E. *Protective Material Coatings for Preserving Cultural Heritage Monuments and Artwork*; Bentham Science Publishers: Singapore, 2022; ISBN 978-981-5049-04-6.

8. Artesani, A.; Di Turo, F.; Zucchelli, M.; Traviglia, A. Recent Advances in Protective Coatings for Cultural Heritage–An Overview. *Coatings* **2020**, *10*, 217. [CrossRef]

9. Kanth, A.P.; Soni, A.K. Application of Nanocomposites for Conservation of Materials of Cultural Heritage. *J. Cult. Herit.* **2023**, *59*, 120–130. [CrossRef]

10. Yimyai, T.; Thiramanas, R.; Phakkeeree, T.; Iamsaard, S.; Crespy, D. Adaptive Coatings with Anticorrosion and Antibiofouling Properties. *Adv. Funct. Mater.* **2021**, *31*, 2102568. [CrossRef]

11. Watkinson, D. Preservation of Metallic Cultural Heritage. In *Shreir's Corrosion*; Elsevier: Amsterdam, The Netherlands, 2010; pp. 3307–3340, ISBN 978-0-444-52787-5.

12. McNamara, C.J.; Breuker, M.; Helms, M.; Perry, T.D.; Mitchell, R. Biodeterioration of Incralac Used for the Protection of Bronze Monuments. *J. Cult. Herit.* **2004**, *5*, 361–364. [CrossRef]

13. Wolfe, J.; Grayburn, R. A Review of the Development and Testing of Incralac Lacquer. *J. Am. Inst. Conserv.* **2017**, *56*, 225–244. [CrossRef]

14. Giuntoli, G.; Rosi, L.; Frediani, M.; Sacchi, B.; Salvadori, B.; Porcinai, S.; Frediani, P. Novel Coatings from Renewable Resources for the Protection of Bronzes. *Prog. Org. Coat.* **2014**, *77*, 892–903. [CrossRef]

15. Giuliani, C.; Pascucci, M.; Riccucci, C.; Messina, E.; Salzano De Luna, M.; Lavorgna, M.; Ingo, G.M.; Di Carlo, G. Chitosan-Based Coatings for Corrosion Protection of Copper-Based Alloys: A Promising More Sustainable Approach for Cultural Heritage Applications. *Prog. Org. Coat.* **2018**, *122*, 138–146. [CrossRef]

16. Masi, G.; Bernardi, E.; Martini, C.; Vassura, I.; Skrlep, L.; Švara Fabjan, E.; Gartner, N.; Kosec, T.; Josse, C.; Esvan, J.; et al. An Innovative Multi-Component Fluoropolymer-Based Coating on Outdoor Patinated Bronze for Cultural Heritage: Durability and Reversibility. *J. Cult. Herit.* **2020**, *45*, 122–134. [CrossRef]

17. Nistor, C.L.; Mihaescu, C.I.; Bala, D.; Gifu, I.C.; Ninciuleanu, C.M.; Burlacu, S.G.; Petcu, C.; Vladu, M.-G.; Ghebaur, A.; Stroea, L.; et al. Novel Hydrophobic Nanostructured Antibacterial Coatings for Metallic Surface Protection. *Coatings* **2022**, *12*, 253. [CrossRef]

18. Chiavari, C.; Balbo, A.; Bernardi, E.; Martini, C.; Bignozzi, M.C.; Abbottoni, M.; Monticelli, C. Protective Silane Treatment for Patinated Bronze Exposed to Simulated Natural Environments. *Mater. Chem. Phys.* **2013**, *141*, 502–511. [CrossRef]

19. Su, Y.; Wang, X.; Zhao, H.; Zhang, C.; Yuan, F.; Guo, J.; Feng, C.; Shen, J. UV Resistance of Sol-Gel Hydrophobic Silica Antireflective Coatings. *J. Sol-Gel Sci Technol.* **2023**, *106*, 381–392. [CrossRef]

20. Ghodrati, M.; Mousavi-Kamazani, M.; Bahrami, Z. Synthesis of Superhydrophobic Coatings Based on Silica Nanostructure Modified with Organosilane Compounds by Sol–Gel Method for Glass Surfaces. *Sci. Rep.* **2023**, *13*, 548. [CrossRef]

21. Chen, C.; Yu, M.; Zhan, Z.; Ge, Y.; Sun, Z.; Liu, J. Effect of PH on the Structure and Corrosion Protection Properties of Sol-Gel Coatings. *Corros. Sci.* **2023**, *212*, 110955. [CrossRef]

22. Adamopoulos, F.G.; Vouvoudi, E.C.; Pavlidou, E.; Achilias, D.S.; Karapanagiotis, I. TEOS-Based Superhydrophobic Coating for the Protection of Stone-Built Cultural Heritage. *Coatings* **2021**, *11*, 135. [CrossRef]

23. Wang, G.; Chai, Y.; Li, Y.; Luo, H.; Zhang, B.; Zhu, J. Sandstone Protection by Using Nanocomposite Coating of Silica. *Appl. Surf. Sci.* **2023**, *615*, 156193. [CrossRef]

24. Dwivedi, D.; Lepková, K.; Becker, T. Carbon Steel Corrosion: A Review of Key Surface Properties and Characterization Methods. *RSC Adv.* **2017**, *7*, 4580–4610. [CrossRef]

25. Figueira, R.; Fontinha, I.; Silva, C.; Pereira, E. Hybrid Sol-Gel Coatings: Smart and Green Materials for Corrosion Mitigation. *Coatings* **2016**, *6*, 12. [CrossRef]

26. Gąsiorek, J.; Szczurek, A.; Babiarczuk, B.; Kaleta, J.; Jones, W.; Krzak, J. Functionalizable Sol-Gel Silica Coatings for Corrosion Mitigation. *Materials* **2018**, *11*, 197. [CrossRef] [PubMed]

27. Bescher, E.; Mackenzie, J.D. Sol-Gel Coatings for the Protection of Brass and Bronze. *J. Sol-Gel Sci. Technol.* **2003**, *26*, 1223–1226. [CrossRef]

28. Stanley-Price, N.; Talley, M.K.; Melucco Vaccaro, A. (Eds.) *Historical and Philosophical Issues in the Conservation of Cultural Heritage*; Readings in conservation; Getty Conservation Institute: Los Angeles, CA, USA, 1996; ISBN 978-0-89236-250-9.

29. Kiele, E.; Lukseniene, J.; Griguceviciene, A.; Selskis, A.; Senvaitiene, J.; Ramanauskas, R.; Raudonis, R.; Kareiva, A. Methyl– Modified Hybrid Organic-Inorganic Coatings for the Conservation of Copper. *J. Cult. Herit.* **2014**, *15*, 242–249. [CrossRef]

30. Masi, G.; Josse, C.; Esvan, J.; Chiavari, C.; Bernardi, E.; Martini, C.; Bignozzi, M.C.; Monticelli, C.; Zanotto, F.; Balbo, A.; et al. Evaluation of the Protectiveness of an Organosilane Coating on Patinated Cu-Si-Mn Bronze for Contemporary Art. *Prog. Org. Coat.* **2019**, *127*, 286–299. [CrossRef]

31. Finšgar, M.; Milošev, I. Inhibition of Copper Corrosion by 1,2,3-Benzotriazole: A Review. *Corros. Sci.* **2010**, *52*, 2737–2749. [CrossRef]

32. Donnici, M.; Ferrari, E.; Neff, D.; Daniele, S. Green Protectives on Corroded Copper Artworks: Surface Characterization and Electrochemical Behaviour in Simulated Acid Rain. *J. Cult. Herit.* **2021**, *51*, 97–106. [CrossRef]

33. Quadri, T.W.; Olasunkanmi, L.O.; Fayemi, O.E.; Ebenso, E.E. Utilization of ZnO-Based Materials as Anticorrosive Agents: A Review. In *Inorganic Anticorrosive Materials*; Elsevier: Amsterdam, The Netherlands, 2022; pp. 161–182, ISBN 978-0-323-90410-0.

34. Ammar, S.; Ramesh, K.; Vengadaesvaran, B.; Ramesh, S.; Arof, A.K. Formulation and Characterization of Hybrid Polymeric/ZnO Nanocomposite Coatings with Remarkable Anti-Corrosion and Hydrophobic Characteristics. *J. Coat. Technol. Res.* **2016**, *13*, 921–930. [CrossRef]

35. Tănase, M.A.; Marinescu, M.; Oancea, P.; Răducan, A.; Mihaescu, C.I.; Alexandrescu, E.; Nistor, C.L.; Jinga, L.-I.; Diţu, L.M.; Petcu, C.; et al. Antibacterial and Photocatalytic Properties of ZnO Nanoparticles Obtained from Chemical versus Saponaria Officinalis Extract-Mediated Synthesis. *Molecules* **2021**, *26*, 2072. [CrossRef]

36. Assaad, H.I.; Zhou, L.; Carroll, R.J.; Wu, G. Rapid Publication-Ready MS-Word Tables for One-Way ANOVA. *SpringerPlus* **2014**, *3*, 474. [CrossRef]

37. Magdaleno-López, C.; De Jesús Pérez-Bueno, J. Quantitative Evaluation for the ASTM D4541-17/D7234 and ASTM D3359 Adhesion Norms with Digital Optical Microscopy for Surface Modifications with Flame and APPJ. *Int. J. Adhes. Adhes.* **2020**, *98*, 102551. [CrossRef]

38. Gu, F.; Wang, S.F.; Lü, M.K.; Zhou, G.J.; Xu, D.; Yuan, D.R. Structure Evaluation and Highly Enhanced Luminescence of Dy^{3+}-Doped ZnO Nanocrystals by Li^+ Doping via Combustion Method. *Langmuir* **2004**, *20*, 3528–3531. [CrossRef] [PubMed]

39. La Russa, M.F.; Rovella, N.; Alvarez De Buergo, M.; Belfiore, C.M.; Pezzino, A.; Crisci, G.M.; Ruffolo, S.A. Nano-TiO_2 Coatings for Cultural Heritage Protection: The Role of the Binder on Hydrophobic and Self-Cleaning Efficacy. *Prog. Org. Coat.* **2016**, *91*, 1–8. [CrossRef]

40. Hafez, I.T.; Biskos, G. New Method for the Protection and Restoration of Calcareous Cultural Heritage Stones by Polyelectrolytes and Hydroxyapatite Nanocrystals. *J. Colloid Interface Sci.* **2021**, *604*, 604–615. [CrossRef]

41. Clare, T.L.; Swartz, N.A. Characterization of High Performance Protective Coatings for Use on Culturally Significant Works. In *Intelligent Coatings for Corrosion Control*; Elsevier: Amsterdam, The Netherlands, 2015; pp. 641–671, ISBN 978-0-12-411467-8.

42. *Artistry in Bronze: The Greeks and Their Legacy: XIX International Congress on Ancient Bronzes*; Daehner, J.; Lapatin, K.D.S.; Spinelli, A.; The J. Paul Getty Museum and Getty Conservation Institute, Eds.; The J. Paul Getty Museum and Getty Conservation Institute: Los Angeles, CA, USA, 2017; ISBN 978-1-60606-542-6.

43. Xue, G.; Wu, P.; Dai, Q.; Cheng, R. The Coupling Mechanism of Benzotriazole Pre-Treated Copper Metal and Epoxy Resin. *Angew. Makromol. Chem.* **1991**, *188*, 51–61. [CrossRef]

44. Moradienayat, M.; González-Benito, J.; Olmos, D. Airbrushed PSF/ZnO Composite Coatings as a Novel Approach for the Consolidation of Historical Bones. *Nanomaterials* **2023**, *13*, 625. [CrossRef]

45. Purcar, V.; Şomoghi, R.; Niţu, S.; Nicolae, C.-A.; Alexandrescu, E.; Gîfu, I.; Gabor, A.; Stroescu, H.; Ianchiş, R.; Căprărescu, S.; et al. The Effect of Different Coupling Agents on Nano-ZnO Materials Obtained via the Sol–Gel Process. *Nanomaterials* **2017**, *7*, 439. [CrossRef] [PubMed]

46. Ghosh, G.; Sidpara, A.; Bandyopadhyay, P.P. Understanding the Role of Surface Roughness on the Tribological Performance and Corrosion Resistance of WC-Co Coating. *Surf. Coat. Technol.* **2019**, *378*, 125080. [CrossRef]

47. Foroozan E, A.; Naderi, R. Effect of Coating Composition on the Anticorrosion Performance of a Silane Sol–Gel Layer on Mild Steel. *RSC Adv.* **2015**, *5*, 106485–106491. [CrossRef]

48. Uc-Fernández, E.; González-Sánchez, J.; Ávila-Ortega, A.; Pérez-Padilla, Y.; Cervantes-Uc, J.M.; Reyes-Trujeque, J.; Talavera-Pech, W.A. Anticorrosive Properties of a Superhydrophobic Coating Based on an ORMOSIL Enhanced with MCM-41-HDTMS Nanoparticles for Metals Protection. *J. Coat. Technol. Res.* **2023**, *20*, 347–357. [CrossRef]

49. Mihelčič, M.; Slemenik Perše, L.; Šest, E.; Jerman, I.; Giuliani, C.; Di Carlo, G.; Lavorgna, M.; Surca, A.K. Development of Solvent- and Water-Borne Fluoropolymer Protective Coatings for Patina-Free Bronze Discs. *Prog. Org. Coat.* **2018**, *125*, 266–278. [CrossRef]

50. D01 Committee. *Test Methods for Rating Adhesion by Tape Test*; ASTM International: West Conshohocken, PA, USA. [CrossRef]

51. Bridgland, J.; International Council of Museums (Eds.) *ICOM-CC: 18th Triennial Conference, Copenhagen, 4–8 September 2017: Linking Past and Future: Preprints*; International Council of Museums: Paris, France, 2017; ISBN 978-92-9012-426-9.

52. Brebbia, C.A. (Ed.) *Materials Characterisation VII.*; WIT transactions on engineering sciences; WIT Press: Southampton: Boston, MA, USA, 2015; ISBN 978-1-84564-948-7.

53. Croll, S.G. Surface Roughness Profile and Its Effect on Coating Adhesion and Corrosion Protection: A Review. *Prog. Org. Coat.* **2020**, *148*, 105847. [CrossRef]